# SIMPLE EULERIAN-LAGRANGIAN EULERIAN-LAGRANGIAN APPROACH TO SOLVE SOLVING EQUATIONS FOR SINKING PARTICULATE ORGANIC MATTER IN THE OCEAN

Vladimir Maderich<sup>1</sup>, Igor Brovchenko<sup>1</sup>, Kateryna Kovalets<sup>1</sup>, Seongbong Seo<sup>2</sup>, and Kyeong Ok Kim<sup>2</sup>

<sup>1</sup>Institute of Mathematical Machine and System Problems, Glushkov av., 42, Kyiv 03187, Ukraine

Correspondence: Kyeong Ok Kim (kokim@kiost.ac.kr)

**Abstract.** A gravitational sinking of the Gravitational sinking of particulate organic matter (POM) is a key mechanism of the vertical transport of carbon in the deep ocean and its subsequent sequestration. The size spectrum of these particles is formed in the euphotic layer by the primary production and various mechanisms, including food web consumption. The mass of masses of the particles, as they descend, changed change under aggregation, fragmentation, bacterial decomposition which depends and bacterial decomposition. These processes depend on the water temperature and oxygen concentration, particle sinking velocity, age ages of the organic particles, ballasting and other factors. In this paperwork, we developed simple Eulerian-Lagrangian approach to solve a simple Eulerian-Lagrangian approach to solving equations for sinking particulate matter when the influence of the size and age of effects of the sizes and ages of the particles, temperature and oxygen concentration on their dynamics and degradation processes were taken into accountare considered. The model considers feedback between the degradation rate and the particle sinking velocity. We rely on the known parameterizations, but our Eulerian-Lagrangian approach to Eulerian-Lagrangian approach for solving the problem differs, allowing which enables the algorithm to be incorporated into biogeochemical global ocean models with relative ease. Two novel analytical solutions of a system of the one-dimensional Eulerian equation for Euler equations for the POM concentration and Lagrangian equations for Lagrange equations for the particle mass and position were obtained for constant and age-dependent degradation rates. At a constant rate of particle sinking , they correspond to exponential and power-law. The feedback between the degradation rate and sinking velocity leads to significant differences in the vertical profiles of the POM concentration. It was found that feedback between degradation rate and sinking velocity results to a significant change in POM and POM flux vertical profiles. The calculations and sinking flux, in contrast to the solutions obtained at a constant sinking velocity, where the concentration and flux profiles of the POM are similar. The calculation results are compared with the available measurement data for the POM and POM flux for the latitude band of 20-30 bands of 20-30 N in the Atlantic and Pacific Oceans and 50-60 S in the Southern Ocean. The dependence of the degradation rate on temperature significantly affected the profiles of POM concentration the POM concentration and sinking flux by enhancing the degradation of sinking particles in the ocean's upper layer and suppressing it in the deep layer of

<sup>&</sup>lt;sup>2</sup>Korea Institute of Ocean Science and Technology, Busan, Republic of Korea

the ocean. The influence of oxygen concentration in all cases considered. In all cases considered, the influence of the oxygen concentration was insignificant compared to that of the distribution of temperature with depth.

Copyright statement. TEXT

## 1 Introduction

25

A gravitational sinking of the Gravitational sinking of particulate organic matter (POM) is a key mechanism of the vertical transport of carbon in the deep ocean (gravitational biological pump) and its subsequent sequestration (Siegel et al., 2023). The biological pump mechanism provides not only the transfer and burial of carbon, but also nutrients, trace metals, and natural and artificial radionuclides through the scavenging mechanism (Roca-Martí and Puigcorbé, 2024; Maderich et al., 2022). —a scavenging mechanism (Roca-Martí and Puigcorbé, 2024; De Soto et al., 2018; Maderich et al., 2022). In addition to the processes of sorption and desorption, the mechanism of scavenging is controlled by the sizes of the sinking particles, their densities, the sinking velocity, and the processes of organic particle degradation (Maderich et al., 2021).

The size spectrum of the sinking particles is formed in the euphotic layer by the primary production and various mechanisms, including aggregation and fragmentation under the influence of mechanical factors (Burd, 2024) and through food web consumption. The mass of masses of the particles, as they descend in deep layers of the ocean, decreases decrease under the influence of grazing by filter feeders and bacterial decomposition, which depends on the water temperature and oxygen concentration (Cram et al., 2018), particle falling velocity (Alcolombri et al., 2021), age ages of the organic particle particles (Jokulsdottir and Archer, 2016; Aumont et al., 2017) and other factors, such as ballasting (Armstrong et al., 2002) (Armstrong et al., 2002; Cram et al., 2018; Maerz et al., 2020). The POM degradation rate can be proportional to the particle volume (DeVries et al., 2014; Cram et al., 2018) or surface area (Omand et al., 2020; Alcolombri et al., 2021).

Many biogeochemical models assume that the settling velocity of particles is constant with depth (e.g., Aumont et al., 2015). Then, depending on the degradation rate, the POM vertical profile can be foundvertical profiles of the POM concentration and sinking flux can be determined. At a constant degradation rate, the corresponding vertical profile of profiles of the particle mass concentration and mass flux will be are exponential (Banse, 1990; Lutz et al., 2002). Assuming that the degradation rate is inversely proportional to the age of particle the particles (Middelburg, 1989), the vertical profile of profiles of the particle mass concentration and mass flux can be found as described by a power law (Cael et al., 2021). This power law corresponds to the well-known empirical "Martin curve" (Martin et al., 1987). However, as the particle mass decreases due to remineralization, the rate at which the particle falls degradation, the sinking velocity also decreases. This feedback, along with other factorsexcept for the age of the particle, is taken into account in several mechanistic models (e.g., DeVries et al., 2014; Cram et al., 2018; Omand et al., 2020; Alcolombri et al., 2021).; however, these models do not consider the ages of the particles.

An analytical solution to the equation for the distribution of POM by particle size was obtained by DeVries et al. (2014) for a constant degradation rate. However, as noted by DeVries et al. (2014), the values of the vertical flux of the POM mass at great depths turned out to be 1-2 were 1-2 orders of magnitude less than observed. It those observed. This discrepancy can be assumed that this discrepancy is to be due to the constancy of the degradation rate with depth in the model. A decrease in the rate of degradation can also be caused by a decrease in water temperature (Cram et al., 2018) and (e.g., Cram et al., 2018) or an increase in the age of ages of the sinking particles with depth.

In this paperwork, we developed simple Eulerian-Lagrangian approach to solve a simple Eulerian-Lagrangian approach for solving equations for sinking particulate matter when the influence of the size and age of effects of the sizes and ages of the particles, temperature and oxygen concentration on their dynamics and degradation processes were taken into account. We rely on the known parameterizations (Kriest and Oshlies, 2008; DeVries et al., 2014; Cram et al., 2018; Omand et al., 2020) are considered. We relied on known parameterizations (Kriest and Oshlies, 2008; DeVries et al., 2014; Cram et al., 2018), but our Eulerian Lagrangian approach to Eulerian Lagrangian approach for solving the problem is different, allowing the model to be incorporated. Our approach involves solving the Euler equation for the concentration of particles of a given size and the Lagrange equations for a sinking organic particle under the influence of microbiological degradation. This enables the incorporation of the proposed algorithm into biogeochemical global ocean models with relative ease. The remainder of the paper is organized as follows: the The equations of the model for sinking particulate organic matter are given in Section presented in Sect. 2. The analytical Analytical solutions for constant and age-dependent degradation rates were are obtained and compared with available data on the vertical concentration and mass flux of the POM in Section-Sect. 3. The numerical Eulerian Lagrangian A numerical Eulerian Lagrangian method for the generalized model is given in Section presented in Sect. 4. The results of the simulations are discussed in Section Sect. 5. Our findings are summarized in Section Sect. 6. The equivalence of the obtained solution and the solution in (DeVries et al., 2014) for a constant rate of degradation is shown in Appendix A.

#### 75 2 Model equations

We consider the vertical flux of the organic particles caused by gravitational forces. Focusing on the development of a numerical Eulerian–Lagrangian method and finding analytical solutions, we limit ourselves to a fairly simple one-dimensional formulation of the problem away from areas of intense currents. The vertical distribution of these particles below the euphotic layer  $z_{eu}$  is governed by the flux of settling particles equilibrated by particle degradation due to bacterial decomposition. The processes of aggregationand fragmentation, fragmentation and ballasting are not included in the model. It is assumed steady state of the particle flux. The Eulerian We limit ourselves to large-scale climatological processes that cover the water column below the euphotic layer to the bottom. We assume that the effects of time variability on the POM flux are relatively small far from this layer, and we consider the steady states of these fluxes.

The Euler particle concentration transport equation and the Lagrangian Lagrange equations for the individual particles are solved. The Euler equation for the POM concentration  $C_{p,d}$  [kg m<sup>-3</sup>] with particle for particles of equivalent spherical

diameter d [m] is written as

$$\frac{\partial W_{p,d}C_{p,d}}{\partial z'} + \gamma C_{p,d} = 0,\tag{1}$$

where  $W_{p,d}$  [m d<sup>-1</sup>] is the settling velocity of a particle of diameter d; z' [m] is the vertical coordinate directed downward downwards from the depth of the euphotic zone ( $z' = z - z_{eu}$ ); and  $\gamma$  [d<sup>-1</sup>] is the degradation rate. The boundary condition for Eq. (1) is

$$z' = 0: \quad C_{p,d} = C_{p,d}(0),$$
 (2)

where  $C_{p,d}(0)$  is a the prescribed POM concentration on at the lower boundary of the euphotic layer  $z_{eu}$ .

We consider the particle dynamics in the Lagrangian coordinate system. The porosity of organic particle aggregates increases with increasing particle size (Mullin, 1966). The relationship between the organic matter mass  $m_d$  and diameter d of porous particles can be parameterized according to the particle fractal dimension

$$m_d = c_m d^{\zeta}. (3)$$

Here,  $\zeta$  ( $\zeta \leq 3$ ) is a dimensionless scaling argument, and  $c_m$  is a prefactor coefficient (Alldredge and Gotschalk , 1988).

The Stokes-type settling velocity  $W_{p,d}$  depends on the density-difference between the density of water and the density of particles the particle, the particle shape, and the kinematic viscosity. To take into account the whole consider the entire ensemble of aforementioned factors that impact the sinkingwe approximated sinking, we approximate the sinking law by power dependence, which is widely used in the particle flux models (e.g. (DeVries et al., 2014))(e.g., DeVries et al., 2014):

$$W_{p,d} = \frac{\partial z'}{\partial t} = c_w d^{\eta},\tag{4}$$

where t is time,  $\eta$  ( $\eta \le 2$ ) is the a dimensionless scaling argument and  $c_w$  [m<sup>1- $\eta$ </sup> d<sup>-1</sup>] is a prefactor coefficient. Note that Figure The measurements of (McDonnell and Buesseler, 2010) show that formulations of sinking velocity as a function of only equivalent particle size can be insufficient because the shapes of the particles (e.g., faecal pellets) can significantly affect the sinking velocity. Fig. 1 from (Cael et al., 2021) also demonstrates the difficulties of describing the sinking speed velocities of particles of various sizes, shapes and structures with a single universal dependence. Therefore, relation Eq. (4) should be considered only as a first approximation in when describing the complex dynamics of particles.

Consider the particle dynamics in the Lagrangian coordinate system. The mass of the particle  $m_d$  is related to the particle diameter d as

$$m_d = c_m d^{\zeta},$$

100

105

110

where  $\zeta$  ( $\zeta \leq 3$ ) is the dimensionless scaling argument and  $e_m$  is a prefactor coefficient (DeVries et al., 2014). Equation (3) takes into account the fact that with an increase in particle size, the porosity of organic particles increases (Mullin, 1966).

We restrict consideration to the case when We consider the case in which the mass of a particle that is descending with velocity  $W_{p,d}$  decreases over time t as a result of microbial degradation. This process can be described by a first-order reaction

with a reaction rate of  $\gamma$  [d<sup>-1</sup>]. The corresponding equation for  $m_d$  [kg] is written as

$$\frac{\partial m_d}{\partial t} = -\gamma(\theta) m_d^{\theta}. \tag{5}$$

Parameter  $\theta = 1$  when the degradation rate is proportional to the particle volume mass, and  $\theta = 2/3$  when the degradation rate is proportional to the surface area of the particle (Omand et al., 2020).

In general ease, the degradation rate depends on many factors. Here we take into account, we consider only several of them: the age of the organic particle t [d], the temperature of the sea water T [°C], and the concentration of oxygen  $[O_2]$  [ $\mu M$ ];

$$\gamma = \gamma(t, T(z'), [O_2](z')). \tag{6}$$

Details of the parameterization The parameterization used in Eq. (6) will be given in Section is presented in detail in Sect. 4.

#### 3 Analytical solutions

140

## 125 3.1 Age-independent degradation rate

First, we consider the case when in which the degradation rate of the particle is age-independent (Age-Independent Degradation age independent (age-independent degradation rate (AID) model). Furthermore, we suppose that the mass loss is proportional to the particle volume mass of the particle ( $\gamma = \gamma_0$ ,  $\theta = 1$ ) and it does not depend on temperature and or oxygen concentration ( $\gamma_0 = \text{const}$ ). Then, the solution of Eq. (5) is

130 
$$m_d = m_{0d} \exp(-\gamma_0 t),$$
 (7)

where  $m_{0d} = c_m d_0^{\zeta}$  is the initial value of particle mass of the particle mass for diameter  $d_0$ . Initially, these particles are the particle is placed at depth z = z'. The diameter of the particle varies with z' = 0. Combining Eq. (7) and Eq. (3) yields the change in the particle diameter over time as

$$d = d_0 \exp\left(-\frac{\gamma_0 t}{\zeta}\right). \tag{8}$$

Assuming the quasi-equilibrium descending Assuming the quasiequilibrium descent of the particle in the Stokes regime-we estimated, as described by Eq. (4), and taking into account that  $W_{p,d} = \partial z'/\partial t$ , we estimate the dependence of  $W_{p,d}$  the particle depth z' on t using Eq. (8):

$$\underline{\underline{W_{p,d}}} = \frac{\partial z'}{\partial t} = c_w d_0^{\eta} \exp\left(-\frac{\eta \gamma_0 t}{\zeta}\right). \tag{9}$$

The vertical path z' travelled by a particle By integrating Eq. (9) from the initial particle depth z' = 0 at t = 0, we find the vertical path travelled by the particle:

$$z' = \frac{\zeta c_w d_0^{\eta}}{\eta \gamma_0} \left[ 1 - \exp\left(-\frac{\eta \gamma_0 t}{\zeta}\right) \right]. \tag{10}$$

Eliminating By eliminating time from Eqs. (9) and (8) by using Eq. (10)we obtain  $W_{p,d}$  and d as the functions of z':

$$W_{p,d} = H(z')c_w d_0^{\eta} (1 - \psi z'), \tag{11}$$

$$d = H(z')d_0 (1 - \psi z')^{\frac{1}{\eta}}, \tag{12}$$

where

145

$$\psi = \frac{\eta \gamma_0}{\zeta c_w d_0^{\eta}} \ge 0. \tag{13}$$

These solutions describe a layer of finite thickness  $h_0 = \psi^{-1}$  below which there are only trivial solutions  $W_{p,d} = d = 0$ . To consider this finding, the Heaviside function is used. The Heaviside function is H(z') = 1 if  $z' \le \psi^{-1}$ , and H(z') = 0 if  $z' > \psi^{-1}$ . Taking into account Eq. (11) we solved, we solve Eq. (1) with the boundary condition in Eq. (2) to obtain

$$C_{p,d} = H(z')C_{p,d}(0)(1-\psi z)^{\frac{\zeta-\eta}{\eta}}$$
 (14)

The solution (14) describes the vertical profile of the POM concentration eaused by for particles of diameter d under the prescribed particle size distribution  $N(d_0)$  [m<sup>-4</sup>] at z' = 0. This distribution can be approximated by power dependence d under the power dependence (e.g., Kostadinov et al., 2009)

155  $N(d_0) = M_0 d_0^{-\epsilon}$ ,

where  $\epsilon$  is a power-law exponent and  $M_0$  is a constant that can be estimated from the total concentration of sinking POM at z'=0. To obtain the size distribution of  $C_{p,d}(0)$ , we use a small increment of particle size  $\Delta d_0$  assuming that under the assumption that the concentration is uniform within the interval  $\Delta d_0$ . Then, the distribution  $C_{p,d}(0)$  as a product of  $N(d_0)$ ,  $m_{0,d}$  and  $\Delta d_0$  is given by

160 
$$C_{p,d}(0) = M_0 d_0^{-\epsilon} m_{0,d} \Delta d_0 = M_0 c_m d_0^{\zeta - \epsilon} \Delta d_0,$$
 (15)

where  $M_0$  is a constant which can be estimated from the total concentration of sinking POM at z' = 0.

The total concentration  $C_p$  is calculated as sum of  $C_{p,d}$  over the sum of concentrations  $C_{p,k}$  in the k-th interval of size d over the total number of  $n_d$  intervals:

$$C_{p}(z') = \sum_{i=0}^{n} \sum_{k=0}^{n} {n_{d} \choose k} C_{p,d,i} c_{p,k} = M_{0} c_{m} \sum_{i=0}^{n} \sum_{k=0}^{n} d_{0,i} c_{0,k} \zeta^{-\epsilon} H(z') (1 - \psi z')^{\frac{\zeta - \eta}{\eta}} \Delta d_{0,i},$$
(16)

where  $d_{0,k} = k\Delta d_0 + d_0^{min}$ ,  $\Delta d_0 = (d_0^{max} - d_0^{min})/n_d$ , and  $d_0^{min}$  and  $d_0^{max}$  are the minimal and maximal values, respectively, of  $d_0$ . At  $\Delta d_0 \to 0$ , the total concentration of sinking POM  $C_p$  [kg m<sup>-3</sup>] in the range from  $d_0^{min}$  to  $d_0^{max}$  can be calculated as

$$C_p(z') = M_0 c_m \int_{d_0^{min}}^{d_0^{max}} \tilde{d}_0^{\xi - \epsilon} H(z') (1 - \psi z')^{\frac{\xi - \eta}{\eta}} d\tilde{d}_0.$$
(17)

Total The total mass flux  $F_p$  [kg m<sup>-2</sup>d<sup>-1</sup>] can be calculated in a similar way:

$$F_{p}(z) = \sum_{i=0}^{n} \sum_{k=0}^{n} C_{p,d,ip,k} W_{p,d,ip,k} = M_{0} c_{m} c_{w} \sum_{i=0}^{n} \left( \sum_{k=0}^{n} d_{0,i0,k} \eta^{+\zeta - \epsilon} H(z') \left( 1 - \psi z' \right)^{\frac{\zeta}{\eta}} \Delta d_{0}.$$

$$(18)$$

170 Here,  $W_{p,k}$  is the sinking velocity in the k-th interval of size d over a total of  $n_d$  intervals.

At  $\Delta d_0 \rightarrow 0$ 

$$F_{p}(z) = M_{0}c_{m}c_{w} \int_{d_{0}^{min}}^{d_{0}^{max}} \tilde{d}_{0}^{\eta + \zeta - \epsilon} H(z') \left(1 - \psi z'\right)^{\frac{\zeta}{\eta}} d\tilde{d}_{0}. \tag{19}$$

The problem for which we obtained the solution (14) for the POM concentration  $C_{p,d}$  is similar to that solved by DeVries et al. (2014) for the particle size spectrum equation. In Appendix A, we show the equivalence of these solutions.

#### 175 3.2 Age-dependent degradation rate

The degradation rate as a function of POM age t [d] can be described by following Middelburg (1989) as

$$\gamma(t) = \frac{\beta}{\alpha + t},\tag{20}$$

where  $\alpha$  [d] and  $\beta$  are empirical constants. We define such a model as an age-dependent degradation rate (ADD) model. The time dependencies for of d and  $W_{p,d}$   $W_{p,d} = \frac{\partial z'}{\partial t}$  with parameterization of the degradation rate Eq. (20) are obtained similarly to those in Section 3.1. They are written as expressed as

$$d = d_0 \left(\frac{\alpha}{\alpha + t}\right)^{\beta/\zeta},\tag{21}$$

$$\underline{W_{p,d}} \frac{\partial z'}{\partial t} = c_w d^{\eta} \left(\frac{\alpha}{\alpha + t}\right)^{\eta \beta / \zeta}.$$
 (22)

The Integrating Eq. (22) from the initial particle depth z'=0 at t=0, we find the path travelled by a sinking particle is as

$$z' = c_w d_0^{\eta} \frac{\alpha \zeta}{\zeta - \eta \beta} \left[ \left( 1 + \frac{t}{\alpha} \right)^{(\zeta - \eta \beta)/\zeta} - 1 \right]. \tag{23}$$

Eliminating time from EqnsBy eliminating time from Eqs. (20), (21) and (22)we obtained depth dependent solutions, we obtain depth-dependent solutions in the same way as in Eqs. (11)-(12):

$$W_{p,d}(z') = c_w d_0^{\eta} (1 + \phi z')^{-\frac{\eta \beta}{\zeta - \eta \beta}}, \tag{24}$$

$$\gamma(z') = \frac{\beta}{\alpha} (1 + \phi z')^{-\frac{\zeta}{\zeta - \eta \beta}}, \tag{25}$$

$$d(z') = d_0 (1 + \phi z')^{-\frac{\beta}{\zeta - \eta \beta}}, \tag{26}$$

190 where

$$\phi = \frac{\zeta - \eta \beta}{\alpha \zeta c_w d_0^{\eta}}.\tag{27}$$

Integrating Eqn By integrating Eq. (1) with a boundary condition the boundary condition in Eq. (2) and taking into account considering Eqs. (24) and (25)we found a we obtain the following solution for  $C_{p,d}$  as:

$$C_{p,d}(z') = C_{p,d_0} \left(1 + \phi z'\right)^{\frac{(\eta - \zeta)\beta}{\zeta - \eta\beta}}.$$
(28)

Assuming that the density of distribution of The density of the distribution of the particle mass concentration at z = 0 is approximated by z' = 0 is assumed to be approximated by a power law (15)we. We can obtain the total concentration of sinking POM  $C_p$  in the range of  $d_0$  from  $d_0^{min}$  to  $d_0^{max}$  as

$$C_p(z') = M_0 c_m \int_{d_0^{min}}^{d_0^{max}} \tilde{d}_0^{\zeta - \epsilon} \left( 1 + \phi z' \right)^{\frac{(\eta - \zeta)\beta}{\zeta - \eta\beta}} d\tilde{d}_0. \tag{29}$$

The corresponding total mass flux  $F_p(z)$  is written as

$$F_{p}(z') = \int_{d_{0}^{min}}^{d_{0}^{max}} W_{p,d} C_{p,d} d\tilde{d}_{0} = M_{0} c_{m} c_{w} \int_{d_{0}^{min}}^{d_{0}^{max}} \tilde{d}_{0}^{\eta + \zeta - \epsilon} (1 + \phi z') \frac{\zeta_{p,d}^{b}}{\zeta_{p,d}^{c}} d\tilde{d}_{0}.$$

$$(30)$$

## 3.3 Comparison of analytical solutions

The obtained analytical solutions have several important properties. At First, we compare these solutions with the solutions obtained under the assumption of a constant sinking velocity  $W_{p,d} = W_p(d_0)$ , the solution of when

 $W_{p,d} = c_w d_0^{\eta}.$ 

205 The solution of Eq. (1) for a constant degradation rate  $\gamma$  corresponds to the exponential profile of the particle concentration

$$C_p(z', d_0) = C_p(0, d_0) \exp\left(-\frac{\gamma_0 z'}{c_w d_0^{\eta}}\right),$$
 (31)

while for whereas the time-dependent degradation rate (20) it corresponds to the power-law distribution of the POM concentration

$$C_p(z', d_0) = C_p(0, d_0) \left( \frac{\alpha c_w d_0^{\eta}}{\alpha c_w d_0^{\eta} + z'} \right)^{\beta}.$$
(32)

Both Both of these solutions are frequently used to approximate observed particle flux profiles, e.g. (Martin et al., 1987) and (Lutz et al., 2002). The corresponding profiles normalized to values at the base of the euphotic layer  $C_p(z_{eu})$  and  $F(z_{eu})$  are shown in Fig. 1 where, (Martin et al., 1987; Lutz et al., 2002). Notably, a solution of the form (32) can alternatively be obtained under the assumption of a constant degradation rate and a linear increase in the sinking velocity (Kriest and Oshlies, 2008; Cael and Bisson

Table 1. The baseline Baseline model parameters.

Parameters	Value/range	Unit	Reference
$\overline{\eta}$	1.17	-	Smayda (1970)
ζ	2.28	-	Mullin (1966)
$\gamma_0$	0.03	$\mathrm{d}^{-1}$	Kriest and Oshlies (2008)
$c_w$	$2.2\cdot 10^5$	$m^{1-\eta}d^{-1}$	Kriest and Oshlies (2008)
$\epsilon$	4.2	-	Kostadinov et al. (2009)
$Q_{10}$	2 - 3	-	Cram et al. (2018)
$T_{ref}$	4	°C	Cram et al. (2018)
$K_O$	8	$\mu$ M	Cram et al. (2018)
$\alpha$	30	d	Aumont et al. (2017)
$\beta$	1	-	Aumont et al. (2017)
$d_0^{max}$	2000	$\mu\mathrm{m}$	DeVries et al. (2014)
$d_0^{min}$	20	$\mu\mathrm{m}$	DeVries et al. (2014)
$n_d$	990	_	DeVries et al. (2014)

 $c_w$ ,  $\epsilon$ ,  $\alpha$ ,  $\beta$ ,  $d_0^{max}$ ,  $d_0^{min}$ , n-and  $n_d$ ) in Table 1 were as chosen by DeVries et al. (2014) and Aumont et al. (2017). As seen the same as in (DeVries et al., 2014) and (Aumont et al., 2017). As shown in Fig. 1, with such parameters these parameters,  $C_p$  and  $F_p$  decay much faster for AID than for the AID model than for the ADD model. Note that Notably,  $C_p$  and  $F_p$  tend to exhibit exponential or power-law profiles only at great depths. At the same time Moreover, at a constant particle velocity, the weighted vertical mass-weighted sinking velocity of particles (Fig. 1c) for both AID and ADD models the speed

$$\overline{W}_p(z') = \frac{F_p(z')}{C_p(z')}$$

220

225

230

increases with depth.

The presence of feedback between  $\gamma$  and  $W_{p,d}$  leads to a significant change in these significant changes in the  $C_p$  and  $F_p$  profiles. In the case of a constant  $\gamma_0$ , the vertical distribution of the concentration  $C_{p,d}$  for one surface fraction of POM size  $d_0$  is limited by a finite layer of thickness  $h_0 = (\zeta c_w d_0^\eta)(\eta \gamma_0)^{-1}$ . Particles The particles in this layer sink at a linearly decreasing velocity. The mass of particles also decreases with depth to a depth where masses of the particles also decrease with depth until a depth at which they are completely remineralized is reached. The size distribution for a single particle at depth z' is  $N(d,z') = C_{p,d}m_d \sim (1-\psi z')^{-1}N(d,z') = C_{p,d}m_d^{-1} \sim (1-\psi z')^{-1}$ . At  $z' \to h_0$ ,  $N(d,z') \to \infty$  while as  $m_d \to 0$ . The finite thickness of the layer of sinking particles with the parameters given in Table 1 varies in the range from 41.3 from 45.4 m at  $d_0 = 20~\mu$ m to 9937 m at  $d_0 = 2000~\mu$ m. Note that Notably, the solution to the problem in a different formulation (Omand et al., 2020) has qualitatively the same the same qualitative character. However, the profiles of total POM concentration and total POM flux decay asymptotically approaching to the exponential exponential profiles, in contrast to the profiles (47.14)

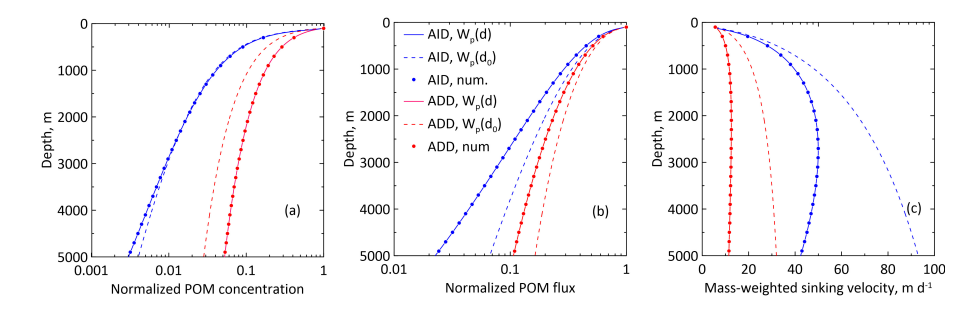


Figure 1. The normalized Normalized total POM concentration  $C_p$  (a), total POM flux  $F_p$  (b), and weighted vertical velocities of the particles (c) for the AID (blue lines) and ADD (red lines) models calculated from the analytical and numerical solutions. The dashed line corresponds lines correspond to the solutions of (1) at constant  $W_p(d_0)$ , while whereas the solid line corresponds to the solution of the problem at variable  $W_{p,d}$ )  $W_{p,d}$ . The small circles correspond to the numerical solutions obtained via the AID and ADD models.

and (1811) for one class of particle sizes  $d_0$  on z'=0. These profiles The total concentration and flux profiles, normalized to values at the base of the euphotic layer, are shown in Fig. 1where, where the  $C_p$  and  $F_p$  profiles were obtained by summation of via the summation of the  $n_d$  profiles in Eqs. (16) and (18). The baseline parameters for calculation are given the calculation are presented in Table 1. These parameter values match those used by DeVries et al. (2014). Therefore, the curves in Fig. 1 also coincide with the corresponding curves in Fig. 1c from (DeVries et al., 2014)calculated using another but, which were calculated using an equivalent formulation of the same problem, as shown in the Appendix.

235

240

245

250

255

In contrast to the AID model solution (16), the POM concentration profile (28) decays asymptotically with depth at  $\zeta > \eta$  and  $\zeta > \eta\beta$  for the ADD model (20). These conditions are met for the parameters listed in Table 1. The rate of degradation  $\gamma$  also decays with depth; the corresponding exponent in (25) differs from the parameter. Unlike the models (Kriest and Oshlies, 2008; Cael and Bisson, 2018) that use the same "Martin curve" power-law dependence (32) for the concentration and mass flux of POM with the exponent  $\beta$  in, the exponent in the obtained solution (28) depends not only on  $\beta$  but also on the parameters that characterize the sinking velocity  $(\eta)$  and the particle mass fractal dimension  $(\zeta)$ .

The sensitivity of the models with a constant sinking rate (32). A sensitivity to the AID model parameters was considered by DeVries et al. (2014). They found that of the four parameters controlling the flux profile reported that four parameters  $(\eta, \zeta, \gamma_0, \text{ and } \epsilon)$ , the most significant control the flux profile and that the most significant factor is the slope of the particle distribution  $\epsilon$  on z'=0, which has the greatest influence on the depth distribution of particles. As follows from the particles. In Fig. 2in which, the variables are presented in logarithmic coordinates, only. Only the vertical distribution of  $C_p$  is close to the power distribution with an exponent of about approximately 1, while whereas the distribution with the depth of the total particle flow depth of  $F_p$  significantly deviates from the power law dependence power law (Martin's law). The sensitivity of the concentration and flux profiles to the values of parameters  $\alpha$  and  $\beta$  parameters is examined in Figure 2. An increase in the parameter  $\alpha$  leads to a deepening of the concentration and particle flux profiles, while whereas an increase in the  $\beta$  leads to a shallowing of these profiles.

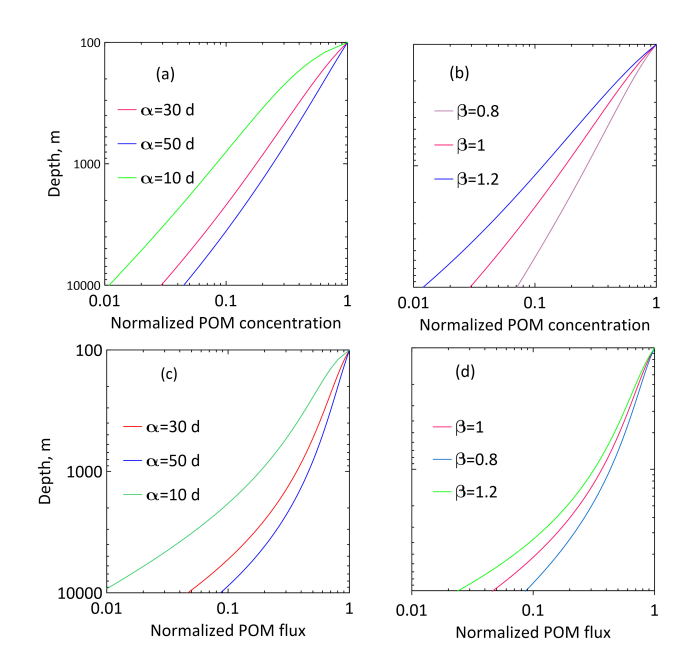


Figure 2. The normalized Sensitivity of the normalised total particle concentration  $C_p$  (a) and total particle flux  $F_p$  (b) sensitivity to parameters  $\alpha$  and  $\beta$ .

The relative maximal absolute errors [%] of the calculated AIDR and ADDR solutions for  $C_p$  and  $F_p$  are presented in Table S1. We compare the solutions at spectral resolutions  $n_d = 100$  and  $n_d = 10$  with the baseline calculation at  $n_d = 990$ . These estimates demonstrate the necessity of fine resolution of the spectre of particles at the lower boundary of the euphotic zone for obtaining accurate profiles of the POM concentration and sinking flux. In this case, the particle concentration profile is more sensitive to the spectral resolution than the sinking flux profile is.

#### 4 Numerical model

260

265

# 4.1 Numerical algorithm

The model discussed in the previous section is based on several simplifying assumptions that made it possible to obtain make obtaining analytical solutions to the system of equations possible. However, when we expand the model to include new important factors in the processes of sinking and remineralization of POM, analytical solutions to the problem can no longer be obtained. Therefore, a numerical Eulerian-Lagrangian approach to solving the new numerical Eulerian-Lagrangian approach for solving this problem was developed.

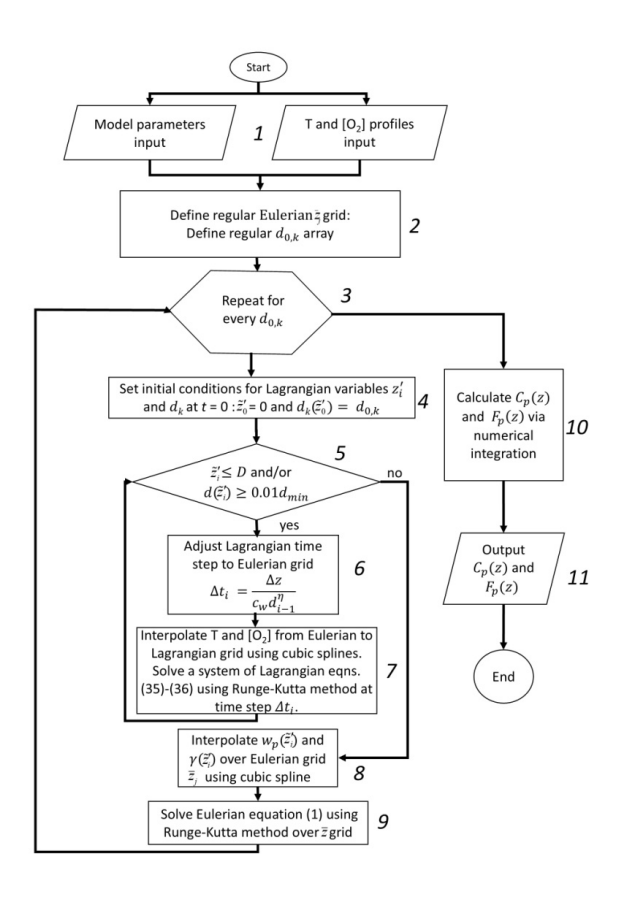


Figure 3. The Eulerian-Lagrangian Eulerian-Lagrangian method flow chart for equations of sinking particulate organic matter.

Here we will limit ourselves to the case where, we consider the case in which the degradation rate depends on the age of the organic particle (ADD model), the temperature of the sea water T and the concentration of oxygen  $[O_2]$ :

$$270 \quad \gamma = \gamma(t, T(z'), [O_2](z')) = \left(\frac{\beta}{\alpha + t}\right) \left(Q_{10}^{\frac{T - T_{ref}}{10}}\right) \left(\frac{[O_2]}{K_O + [O_2]}\right), \tag{33}$$

where  $Q_{10}$  is the temperature coefficient,  $T_{ref}$  is a reference temperature,  $K_{O2}$  (kg m<sup>-3</sup> and  $K_{O}$  [ $\mu$ M] is an oxygen dependence parameter (Cram et al., 2018). When  $\gamma$  does not depend on age (AID model)then, then

$$\gamma = \gamma_0 \left( Q_{10}^{\frac{T - T_{ref}}{10}} \right) \left( \frac{[O_2]}{K_O + [O_2]} \right)_{\underline{!}}. \tag{34}$$

The system of Lagrangian Lagrange equations for particle depth and size derived from Eqs. (4)-(5) is as follows:

$$\frac{\partial d}{\partial t} = -\frac{\gamma(t, T(z'), [O_2](z')}{\zeta} \frac{\gamma(t, T(z'), [O_2](z'))}{\zeta} d, \tag{35}$$

$$\frac{\partial z'}{\partial t} = c_w d^{\eta}. ag{36}$$

The initial conditions are that at t = 0: z' = 0 and  $d = d_{0.i}t = 0$ : z' = 0 and  $d = d_{0.i}$ .

The procedure of finding for determining the profiles of  $C_p(z')$  and  $F_p(z')$  is as presented in Fig. 3. It includes 11 steps.

Step 1 The model parameters and temperature and oxygen concentration profiles are read from the input files.

- Step 2 The  $\Delta$  regular Eulerian grid  $\bar{z}'$  is set up established from 0 to the ocean depth D on with  $n_z$  equal intervals  $\Delta z$  with levels  $\bar{z}' = j \cdot \Delta z$ , where  $j = (0, n_z)$ . The particle size spectrum at the lower boundary of the euphotic layer is divided on into  $n_d$  equal intervals of size  $\Delta d$  in the range from  $d_{min}$  to  $d_{max}$ . For every particles size  $d_{0,k}$ ,  $k = (0, n_d)$ .
  - Step 3 Sequential steps 4-9 Steps 4-9 are performed for every  $d_{0,k}$ , where  $k = (0, n_d)$ . Then move to the Step 10., Step 10 is performed.
- 285 Step 4 Set the initial conditions for The initial conditions are set for the Lagrangian particle depth  $\tilde{z_k}'(t_i)$  and size  $d = d_{0,k}$  equations at  $t_i = 0$ .
  - Step 5 If the Lagrangian particle depth  $\tilde{z_k}'(t_i)$  is equal to or greater than the ocean depth D and/or particle diameter on or the particle diameter at this depth level  $d = d_{0,k}$  is equal to or less than 1% of minimum diameter size the minimum diameter  $d_{min}$  then perform. Step 8 else performed; otherwise, Step 6 is performed.
- 290 Step 6 The timescale is divided on the into intervals  $\Delta t_i$ ,  $i = (0, n_t)$  over which equations Eqs. (35)-(36) are integrated. To align the resulting  $\tilde{z_k}'(t_i)$  and regular depth grid  $\bar{z}'$ , the *i*-th timestep duration is calculated as  $\Delta t_{i,k} = \Delta z/(c_w d_{i,k}^{\eta})$ .
  - Step 7 Using the The Lagrangian formulation with respect to time t solve a is used to solve the system of equations (35)-(36) using Runge-Kutta's via the Runge-Kutta method of the 4th order. The cubic Cubic spline interpolation is used to calculate the temperature and oxygen concentration at  $\tilde{z_k}'(t_i)$ .
- 295 Step 8 The  $w_p(\tilde{z_k}'(t_{i+1}))$  and  $\gamma(\tilde{z_k}'(t_{i+1}))$  profiles at on the Lagrangian grid of are interpolated using are interpolated via a cubic spline over the Eulerian grid  $\bar{z}'$ .
  - Step 9 The  $C(p,d)(\bar{z}')$   $C_{p,d}(\bar{z}')$  is calculated by solving Eulerian the Euler equation (1) with Runge-Kutta via the Runge-Kutta method over the regular grid  $\bar{z}'$ . Then move to Step 3., Step 3 is performed.
  - Step 10 The total POM concentration  $C_p(\bar{z}')$  and POM flux  $F_p(\bar{z}')$  are obtained via numerical integration of  $S(p,d)(\bar{z}')$  and  $w_p(\bar{z}')$  by using the composite Simpson-3 rule.
  - Step 11 Model output: The model outputs the total POM concentration  $C_p(\bar{z}')$  and POM flux  $F_p(\bar{z}')$ .

The code for the proposed algorithm, along with the data used in this study, is archived on Zenodo (Kovalets et al., 2025a, b).

## 4.2 Numerical model setup

The simulations Simulations were carried out for the water column of depth a water column with a depth of D=5000 m,  $n_z=1000$ , and  $\Delta z=1$  m. We calculated the vertical profiles of the POM concentration  $C_p$  and flux  $F_p$  using AID and ADD models for the degradation rate. The rest of the remaining model parameters, except with the exception of  $\eta$ , were adopted from Table 1. In Fig.1 the The profiles of  $C_p$  and  $F_p$  were calculated using an above algorithm and via the above algorithm with  $\eta=1.17$  to be compared with analytical solutions for for comparison with the analytical solutions with the AID and ADD parameters from Table 1. As seen in the figure shown in Fig. 1, the numerical and analytical profiles coincide.

The calculations calculation results were compared with the available measurement data for  $C_p$  and  $F_p$  for the latitude 310 band of 20-30 bands of 20-30 N in the Atlantic and Pacific Oceans and 50-60 S of in the Southern Ocean. These calculations aimed to assess the relative influence effects of the vertical distribution distributions of temperature and oxygen in the Atlantic, Pacific and Southern oceans on profiles Oceans on the profiles of  $C_p$  and  $F_p$ . For the Atlantic Ocean, the  $C_p$ and  $F_p$  data are compiled in (Aumont et al., 2017) and (Lutz et al., 2002) while for For the Pacific Ocean, they are given these values are presented in (Martin et al., 1987) and (Druffel et al., 1992). The Southern Ocean data for the Pacific and 315 Atlantic sectors are given presented in (Aumont et al., 2017) and (Lutz et al., 2002). The required for calculations averaged calculations required for averaging over the region and time profiles of T and  $[O_2]$  were constructed using performed with the measurement data from (Boyer et al., 2018). These averaged profiles are shown in Fig. S1 in the Supplement. It is necessary to emphasize the Notably, there is great uncertainty not only in the choice of model parameter values but also in the processes' parameterization parameterization of the processes. This is explained by both an insufficient understanding of the physical and 320 biogeochemical processes - and the lack of a sufficient number of measurements in the deep layers of the ocean. In particular, the observation results (Cael et al., 2021) show large deviations in the parameters of the sinking velocity-particle velocity-particle size relationship (4). In the recent models, the parameter  $\eta$  varies in range has varied from 0.26 (Alcolombri et al., 2021) to 2 (Omand et al., 2020). Therefore in simulations we compare effect, in the simulations, we compared the effects of  $\eta$  on the  $C_p$  and  $F_p$  profiles for two values:  $\eta = 1.17$  (Smayda, 1970) and  $\eta = 0.63$  (Cael et al., 2021). 325

## 5 Modelling results

330

335

340

# 5.1 Comparison of simulations with measurements

Figures  $\frac{4-6}{4-6}$  show the profiles of  $C_p$  and  $F_p$  normalised normalized to  $C_p(z_{eu})$  and  $F_p(z_{eu})$ . They were calculated using the numerical algorithm described in Section Sect. 4.1. These profiles are compared with normalised normalized measurements in the subtropical zones of the Atlantic and Pacific oceans, and also (Fig. 4) and Pacific (Fig. 5) Oceans and in the Atlantic and Pacific sectors of Southern Ocean to consider the Southern Ocean (Fig. 6) to consider the effects of temperature and oxygen concentration effects on POM. When the modelling results are compared with the measurement data, the significant scatter of the measurement data presented in Figs. 4–6 must be noted. This scatter is due both to the difficulties of measuring the concentration and flux of particles and to regional differences in the influx of particles and in the surrounding ocean.

The  $C_p$  and  $F_p$  profiles in Figures 4-64-6 were obtained for three variants of the degradation model. In the first variant (plots a and d),  $C_p$  and  $F_p$  do not depend on the oxygen concentration, and in the third variant (c, f) and f), they depend on temperature, the temperature and oxygen concentration. The first variant is described by analytical solutions for the AID and ADD models. The features of these solutions are discussed in Section 3.3. The profiles of  $C_p$  and  $F_p$  are sensitive to the value of  $\eta$ . The solutions with  $\eta = 0.63$  decay slower than obtained for more slowly than those with  $\eta = 1.17$  as follows also from analytic solutions do, as shown by the analytic solutions in Figs. 4a, 4d, 5a, 5d, 6a, and 6d.

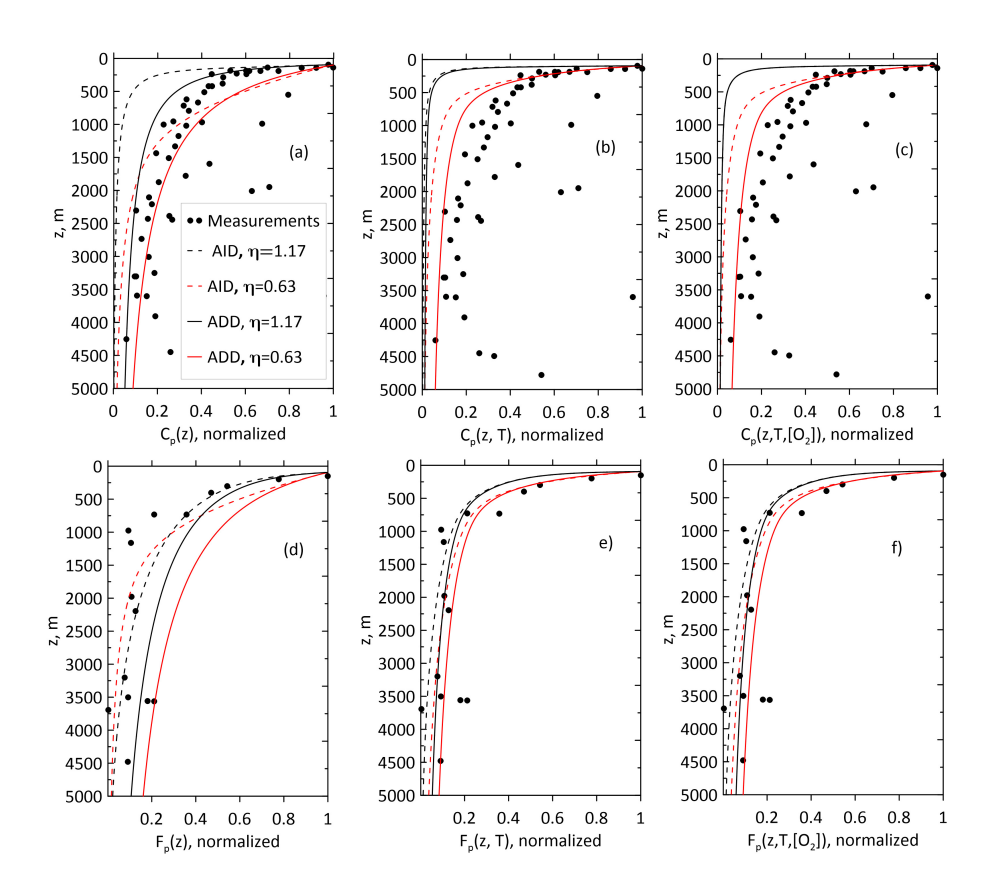


Figure 4. The normalized Normalized total POM concentration  $C_p$  (a-ea-c) and total POM flux  $F_p$  (d-fd-f) versus measurement data in the Atlantic Ocean at 20-30°N (Aumont et al., 2017; Lutz et al., 2002). Three columns of panels correspond to the model without dependency of temperature and oxygen (panels a and d), additional temperature dependence (panels b and e), and both additional dependencies (panels c and f).

Using The use of the AID model leads led to a more rapid decay of  $C_p$  with depth than was observed in all the ocean profiles. At the same time, the decay of  $F_p$  with depth occurs more slowly in most of the measured profiles. The using of ADD model (Figs. 4-6) results in more smooth profiles, howeverqualitatively Moreover, the application of the ADD model resulted in smoother profiles in all oceans; however, the AID and ADD profiles are elose.

345

350

As can be seen from Fig. 4-6, qualitatively close. As shown in Figs. 4b, 4e, 5b, 5e, 6b, and 6e, the dependence of the degradation rate on temperature significantly affected the profiles of  $C_p$  and  $F_p$  enhancing profiles; namely, it enhanced the degradation of sinking particles in the upper layers of the ocean and suppressing suppressed it in the deep layers of the ocean. The influence of the oxygen concentration in all eases considered the cases considered (Figs. 4c, 4f, 5c, 5f, 6c, and 6f) was less significant compared to than that of the distribution of temperature with depth. Overall, including temperature and concentration dependence in the degradation rate relationship improves improved the agreement with ocean measurements. The normalized Mean Bias Errors (MBE) when taking into account mean bias errors (MBEs) when considering the dependence of

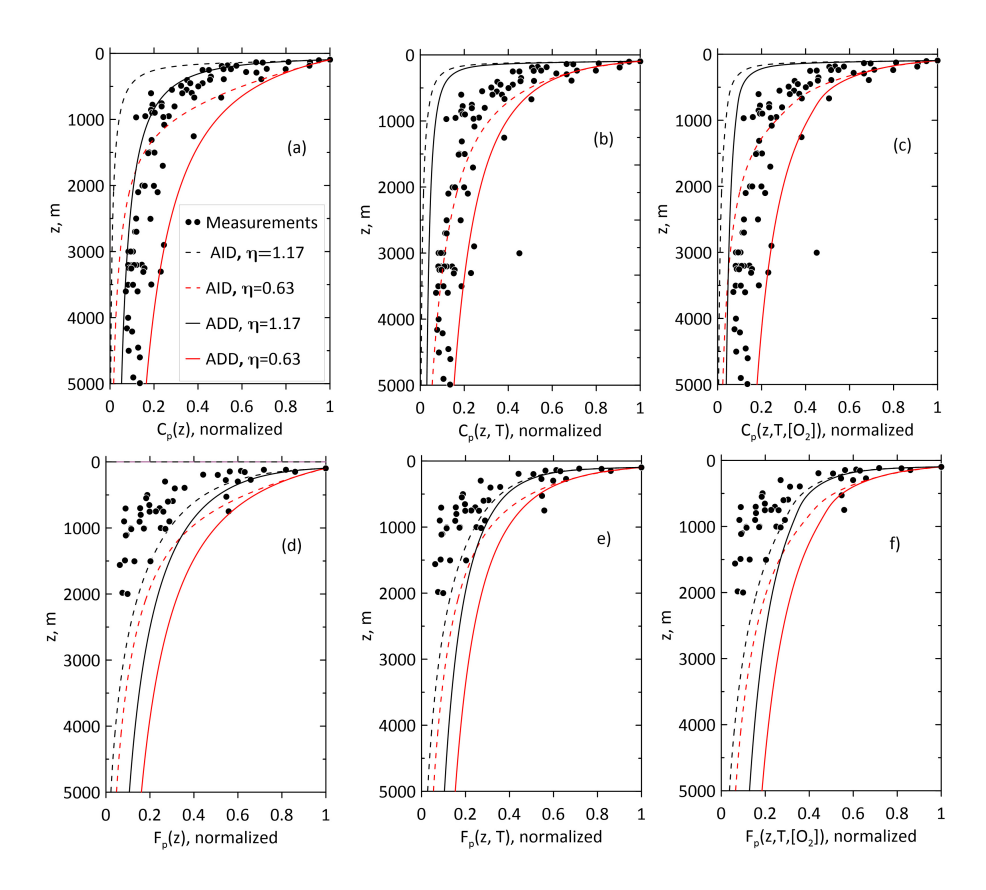


Figure 5. The normalized Normalized total POM concentration  $C_p$  (a-ea-c) and total POM flux  $F_p$  (d-fd-f) versus measurement data in the Pacific Ocean at 20-30°N (Martin et al., 1987; Druffel et al., 1992). Three columns of panels correspond to the model without dependency of temperature and oxygen (panels a and d), additional temperature dependence (panels b and e), and both additional dependencies (panels c and f).

the degradation rate on temperature and oxygen concentration (third variant) are reduced decreased from 9% to -3% compared to first variant those of the first variant, when this dependence was not taken into account. For third variant the Root Mean Square Deviation considered. For the third variant, the root mean square deviation (RMSD) decreased by half comparatively with compared with that of the first variant. Notice that both

355

360

Notably, both the AID and ADD models somewhat underestimates underestimated  $F_p$  when the dependence on temperature is taken into account. As follows from Figs. 4-6was considered. As shown in Figs. 4-6, the use of a AID model leads the AID model led to a more rapid decay of  $S_p$  and  $C_p$  with depth than was observed in all ocean profiles. At the same time Moreover, the decay of  $F_p$  with depth occurs occurred more slowly in most of the measured profiles. The using of use of the ADD model (Figs. 4-6) results in more smooth profiles, however qualitatively 4-6) resulted in smoother profiles; however, qualitatively, the AID and ADD profiles are close, similar. Notably, profiles  $C_p$  and  $F_p$  in Fig. 3c, 3f and 4c, 4f are quite close despite the differences between the temperature and oxygen concentration profiles in the 20-30°N band of the Atlantic and Pacific Oceans

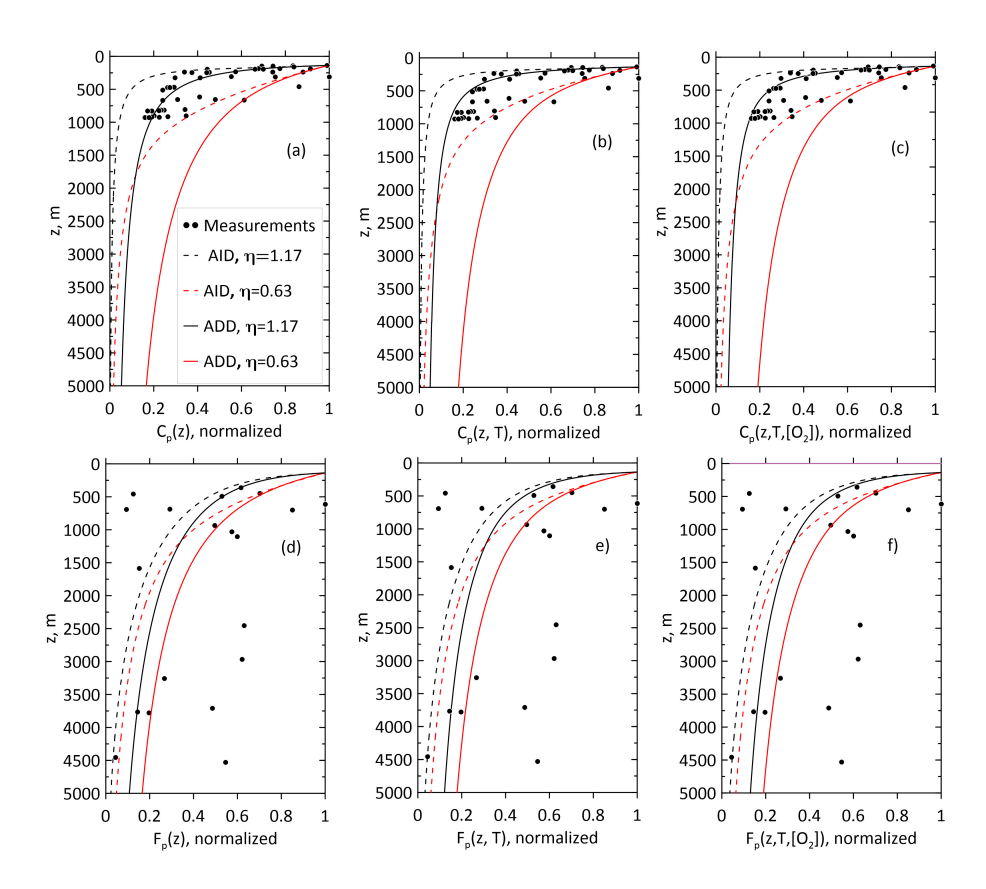


Figure 6. The normalized Normalized total POM concentration  $C_p$  (a-ea-c) and total POM flux  $F_p$  (d-fd-f) versus measurement data in the Southern Ocean at 50-60°N (Aumont et al., 2017; Lutz et al., 2002). Three columns of panels correspond to the model without dependency of temperature and oxygen (panels a and d), additional temperature dependence (panels b and e), and both additional dependencies (panels c and f).

(Fig. S1a-S1b). These profiles in the colder, oxygen-saturated waters of the Southern Ocean (Fig. S1c) attenuate more slowly with depth.

As follow from Fig. 4-6

# 5.2 Sensitivity study

365

370

As shown in Figs. 4–6, the model output was sensitive to the parameters with high uncertainty, such as  $\eta$ . Therefore, a sensitivity study was carried out for the model parameters in Table S1. We used the one-at-a-time method to quantify the effect of the variation of variation in a given parameter on the model output while all other parameters were kept at their initial values (Hamby, 1994; Lenhart et al., 2002; Soares and Calijuri, 2021). The effects of variations in these parameters were estimated for the particle transfer efficiency (TE). Define  $TE_{1000}$  is defined as the ratio of the concentration of POM POM flux at the lower level of the cuphotic layer  $z_{eu}$  to the concentration flux at the lower boundary of the mesopelagic layer z = 1000,

and  $TE_{5000}$  is defined as the ratio of the concentration of POM POM flux at the lower level of the euphotic layer to the concentration flux in the bottom layer at z = 5000m.

The range for parameters is defined as follows: The ranges for the parameters were defined for a constant ratio r > 1. The minimum parameter value  $p_{min}$  was set to be proportional to the reference value  $p_{ref}$  with a ratio value 1/r < 1 and of 1/r, whereas the maximum value  $p_{max}$  was set to be proportional to the reference value  $p_{ref}$  with a ratio value r > 1 to the reference value. For all of r. For the parameters in Table S1, the value of r was chosen to be the same (r = 1.25). This value satisfies to, which satisfies the ranges of all parameters, the parameters.

The model output sensitivity was estimated using a sensitivity index (SI) defined as

$$SI = \frac{TE(p_{max}) - TE(p_{min})}{TE(p_{ref})},$$
(37)

where  $TE(p_{max})$ ,  $TE(p_{min})$  and  $TE(p_{ref})$  are the simulation results for the maximal  $p_{max}$ , minimal  $p_{min}$ , and reference  $p_{ref}$  parameter values, respectively. Calculations of SI were carried out for the Pacific Ocean for the AID and DDR models using with the reference, maximal and minimal values of the parameters from Table  $\frac{S1}{S2}$ .

The sensitivity index  $\overline{TE_{1000}}$  SI( $\overline{TE_{1000}}$ ) is shown in Fig. S2 in the Supplement for the parameters of the AID model. As seen shown in the figure,  $\overline{TE_{1000}}$  SI( $\overline{TE_{1000}}$ ) was most sensitive to the exponent  $\zeta$  in the power law dependence of the particle mass on the particle size (43) and to the exponent  $\epsilon$  in the power law dependence of the particle size distribution at the lower boundary of the euphotic layer (4315). The sign of the index shows if the model reacts indicates whether the model reacted codirectionally to the input parameter change, i.e., if whether the parameter increase/decrease corresponds to the corresponded to an increase/decrease of in the model output parameter. The nature of the dependence of  $TE_{1000}$  on  $\zeta$  and  $\epsilon$  is different. The increase was different. An increase in  $\zeta$  results resulted in an increase in  $TE_{1000}$ , i.e., an increase in the mass of a particle increases increased the transfer efficiency. At the same time, the increase Moreover, an increase in  $\epsilon$  results resulted in a decrease in  $TE_{1000}$ , i.e., an increase in the slope of the spectral particle size distribution leads led to a decrease of in the transfer efficiency. The dependence of  $TE_{1000}$  on  $T_{ref}$  and  $K_O$  was weak (SI << 1), whereas the dependence on  $\gamma_0$ ,  $\eta$  and  $Q_{10}$  was moderate. The sensitivity index  $SI(TE_{5000})$  for the parameters of the AID model is shown in Fig. S3. As seen shown in the figure, it is qualitatively similar to that in Fig. S2. Four parameters ( $\gamma_0$ ,  $\gamma_0$ ,  $\gamma_0$ ,  $\gamma_0$ ,  $\gamma_0$ , and  $\varepsilon$ ) showed strong sensitivity.

The sensitivity index  $TE_{1000}$  for  $SI(TE_{1000})$  values for the parameters of the ADD model is are shown in Fig. S4. Similarly, Similar to the results in Fig. S2.—,  $TE_{1000}$  is was most sensitive to  $\zeta$  and  $\epsilon$ , however, amplitudes of  $TE_{1000}$  are less than; however, the amplitudes of  $SI(TE_{1000})$  were less than those for AID model. The dependence on sensitivity of the ADD model parameters ( $\alpha$  and  $\beta$ ) are was moderate. The sensitivity index  $TE_{5000}$  for  $SI(TE_{5000})$  values for the parameters of the ADD model is are shown in Fig. S5. It similar to the  $TE_{1000}$  Similar to  $SI(TE_{1000})$  for this model, but the amplitudes of  $TE_{5000}$  are greater than  $TE_{1000}$  amplitudes. More details of the magnitudes of the  $SI(TE_{5000})$  values were greater than the magnitudes of the  $Si(TE_{5000})$  values. Additional details on the sensitivity study are given presented in the Supplement.

In this paper

380

385

390

395

## 6 Discussion and conclusions

435

440

In this work, we considered simple Eulerian-Lagrangian approach to solve equations describing a simple Eulerian-Lagrangian approach for solving equations that describe the gravitational sinking of organic particle under influence of the size and age of particles under the effects of the sizes and ages of the particles, temperature and oxygen concentration on their dynamics 410 and degradation processes. The novel In contrast to other approaches, our approach does not use particle spectrum equations (e.g., DeVries et al., 2014) explicitly or power-law particle size distribution assumptions (e.g., Kriest and Evans, 1999; Maerz et al., 2020) . Unlike (Omand et al., 2020), we do not assume a priori the constancy of the particle flux in depth in steady state. Instead, solutions are found for the Euler equation for the concentration of particles of a given size and the Lagrange equations for a 415 sinking organic particle under the influence of microbiological degradation. In the stationary case, the problem is reduced to solving a system of ordinary differential equations of the first order, in contrast to (DeVries et al., 2014), where the solution of the hyperbolic equation of the first order for the particle distribution is found. In addition, the total concentration and flux of the POM are found by summation over the particle distribution at z'=0, whereas in (DeVries et al., 2014) the summation is carried out over all depths. Our approach makes the particle transport model compatible with large-scale biogeochemical 420 models and provides an opportunity to solve the non-stationary problem in the future using Eq. (1) complemented by the time derivative of  $C_{n,d}$  and necessary parameterizations of the POM sinking processes.

Novel analytical solutions of the system of the one-dimensional Eulerian equation for the POM concentration and Lagrangian equations for the particle mass and depth were obtained for constant and age-dependent degradation rates. It was found that feedback between The feedback between the degradation rate and sinking velocity results to a significant change in POM and POM in significant changes in the POM concentration and flux profiles. In the case of a constant  $\gamma_0$  (AID model), the vertical distribution of the concentration  $C_{p,d}$  for a single fraction of the POM size  $d_0$  at  $z_{eu}$  is limited by a finite layer, unlike the exponential profile of the particle concentration that corresponds to a constant sinking velocity. Particles in this such a finite layer sink at a linearly decreasing velocity. At the same time, the distribution of Moreover, the distributions of the total particle concentration  $C_p$  and flux  $F_p$  approaches exponential approach exponential trends with depth for increase of increasing  $d_0$  fractions.

In contrast to those for the AID model, the vertical distribution of distributions of the concentration and vertical velocity decay asymptotically with depth for the ADD model. The rate of degradation in Eulerian variables decays with depth, however ates of degradation of the Eulerian variables decay with depth; however, the corresponding exponent depends not only on the parameter  $\beta_{as}$ , as in the models with a constant sinking velocity (Cael et al., 2021), but also on the parameters characterizing that characterize the vertical velocity of particles  $\eta$  and their porosity  $\zeta$ . With baseline parameters of the particles. With the baseline parameters, the vertical distribution of  $C_p$  is close to the power distribution with an exponent of about approximately 1, while whereas the distribution with the depth of the total particle flow  $F_p$  significantly deviates deviates significantly from the power law dependence ("Martin<sup>2</sup>'s law"). Direct comparison with other models is difficult owing to differences in the parameterizations of processes, with the exception of the model (DeVries et al., 2014) for which the solutions of the equations for the particle spectrum and concentration are established (Appendix A).

A new Eulerian-Lagrangian numerical approach to Eulerian-Lagrangian numerical approach for solving the problem in general cases was presented. It allows to include in consideration of The algorithm includes time steps for Lagrangian variables (sinking velocity and particle mass) and Eulerian depth steps for the concentration of particles of size d. This enables the inclusion of different parameterizations of interacted interacting degradation and sinking processes (e.g., DeVries et al., 2014; Cram et al., I however, here in this study, we limited ourselves to the case where the degradation rate depends on the age of the organic particle, the temperature of the sea water and the concentration of oxygen. The Notably, the developed numerical algorithm is suitable for arbitrary dependencies of mass and sinking velocity on the particle diameter. The proposed numerical method was tested on the obtained analytical solutions.

445

450

455

460

465

The ealculations are calculation results were compared with the available measurement data for the POM and POM flux fluxes for the latitude band of 20-30 bands of 20-30 N in the Atlantic and Pacific Oceans and 50-60 50-60 S in the Southern Ocean. The dependence of the degradation rate on temperature significantly affected affects the profiles of the total particle concentration and flux enhancing significantly; it enhances the degradation of sinking particles in the upper layers of the ocean and suppressing suppresses it in the deep layers of the ocean. Overall, including temperature and concentration dependence in the degradation rate relationship improves the agreement with ocean measurements. In particular, the normalized MBEs when taking into account considering the dependence of the degradation rate on temperature and oxygen concentration are-were reduced from 9% to -3% compared to cases when with cases in which this dependence was not taken into account. Similarly, on the average, average, the RMSD decreased by half when taking into account temperature stratification temperature stratification was considered.

Discrepancies between The discrepancies between the model predictions and observations are were caused by incomplete description descriptions of processes and uncertainty of uncertainties in model parameters, as well as variability of in the measured POM concentration profiles due and flux profiles owing to vertical and horizontal variability of in the ocean fields. We used the one-at-a-time method to quantify the effect of the variation of one the parameter from parameter from the set  $(\gamma_0, \eta, \zeta, \epsilon, T_{ref}, Q_{10}, K_0, \alpha, \beta)$  on the model outputwhile, with all other parameters were kept at their initial values. The effects of variations in these parameters were estimated for on the particle transfer efficiency TE as ratio of POM flux on were estimated as the ratio of the POM flux at  $z_{eu}$  to value on the the value at a depth of 1000 m or 5000 m. The model output sensitivity was estimated using a via the sensitivity index SI (37). Calculations for the Pacific Ocean showed revealed that  $TE_{1000}$  and  $TE_{5000}$  are most sensitive to the parameters  $\zeta$  and  $\epsilon$  respectively, for both models. Therefore, calibration and optimization of these parameters should be primarily carried out, calibrated and optimized. Therefore, it was important to assess the sensitivity of the calculations to the values of the model parameters.

470 It should be noted that Notably, to obtain analytical solutions and demonstrate the numerical Euler-Lagrangian Eulerian-Lagrangian approach, significant simplifications were made in the description of the particle dynamics. In particular, the particle sinking velocity was described in the Stokes approximation—. The aggregation and fragmentation of particles, mineral ballasting, ocean density stratification, and temporal changes in particle flows were not taken into account considered. While some simplifications can be eliminated by using a numerical approach, others require significant generalization. This particularly applies applies particularly to the description of particle ballasting mechanisms. On the one hand, ballast affects the sinking

of particles, but on the other hand, ballast minerals can protect organic matter from remineralization (Cram et al. 2018). In addition, the mechanisms regulating the distribution of particles of different nature between aggregates and free particles are also unclear. These circumstances did not allow the inclusion of ballasting parameterizations in the present model degradation ((Cram et al., 2018)). The processes of fragmentation and consumption of sinking particles, which are important in the upper mesopelagic layer, are poorly understood (Burd, 2024). Comparison of calculation results for different parameter values (e.g.  $\eta$ ) did not reveal the advantage of one parameter value for both  $C_p$  and  $F_p$ , which may be due to the incompleteness of the description of the processes of the simplified model used. Therefore, for the effective application of the proposed approach in biogeochemical models, a parameterization of the main process controls of the biological carbon pump mechanism based on data from natural and laboratory measurements is necessary.

485 *Code and data availability.* The exact version of the model that was used to produce the results presented in this paper is archived on Zenodo (Kovalets et al., 2025a),

and the input data that were used to run the model and generate the plots for all the simulations presented in this paper were obtained from (Kovalets et al., 2025b).

## Appendix A: Derivation of the spectral solution for the size distribution (DeVries et al., 2014)

Herewe will show that , we show that the analytical solution (14) for  $C_{p,d}$  is equivalent to the solution (8) from (DeVries et al., 2014) of the spectral equation for the particle size distribution. To find the particle size distribution at z' we first re-arrange equation, we first rearrange Eq. (12) obtaining the relation to obtain the relationship between  $d_0$  and d at depth z':

$$d_0 = d(1 + \psi z')^{1/\eta}. (A1)$$

The size distribution N(d,z) [m<sup>-4</sup>] is related with to  $C_{p,d}$  and  $m_d$  as

495 
$$C_{p,d} = Nm_d \Delta d_{\underline{\cdot}},$$
 (A2)

where  $\Delta d$  is a small size increment. Combining Eqs. (14), (4), (12), and (A2) gives yields

$$N(d,z') = \frac{C_{p,d}}{m_d \Delta d} = \frac{\Delta d_0}{\Delta d} M_0 d_0^{-\epsilon} \left( 1 + \frac{\eta \gamma_0}{\zeta c_w d^{\eta}} z' \right)^{\frac{\eta - \epsilon}{\eta}}. \tag{A3}$$

In At the limit of  $\Delta d \rightarrow 0$  we obtained, we obtain

$$\lim_{\Delta d \to 0} \frac{\Delta d_0}{\Delta d} = \frac{d}{dd} d_0 = \left( 1 + \frac{\eta \gamma_0}{\zeta c_w d^{\eta}} z' \right)^{\frac{1-\eta}{\eta}}.$$
(A4)

500 Then Eqn, Eq. (A3) can be written as

$$N(d,z') = M_0 d^{-\epsilon} \left( 1 + \frac{\eta \gamma_0}{\zeta c_w d^{\eta}} z' \right)^{\frac{1-\epsilon}{\eta}}.$$
 (A5)

This solution for N coincides with that found obtained by DeVries et al. (2014).

Author contributions. VM-conceptualization; VM and IB-methodology; KK and KOK-software; SS-visualization; KOK, KK, and SS-investigation; VM, IB, and KK-writing (original draft); KOK and SS-writing (review and editing); and VM-supervision. All authors contributed to the interpretation of the findings and the writing of the paper.

Competing interests. The corresponding author declares that none of the authors have any competing interests.

Acknowledgements. The research is supported by the National Research Foundation of Ukraine (project no. 2023.03/0021, and.), the Korea Institute of Marine Science and Technology Promotion (KIMST) funded by the Ministry of Oceans and Fisheries (RS-2023-00256141) and, the European Union's Horizon 2020 research and innovation framework program (PolarRES, Grant Agreement 101003590).

#### 510 References

525

- Alcolombri, U., Peaudecerf, F.J., Fernandez, V.I. Lars-Behrendt, L., Lee K. S., and Stocker, R.: Sinking enhances the degradation of organic particles by marine bacteria, Nat. Geosci. 14, 775–780. https://doi.org/10.1038/s41561-021-00817-x, 2021.
- Armstrong, R.A., Lee, C., Hedges, J.I., Honjo, S., and Wakeham, S.G.: A new, mechanistic model for organic carbon fluxes in the ocean based on the quantitative association of POC with ballast minerals, Deep-Sea Res. II, 49, 219–236219–236, 2002.
- Aumont, O., Ethé, C., Tagliabue, A., Bopp, L., and Gehlen, M.: PISCES-v2: an ocean biogeochemical model for carbon and ecosystem studies, Geosci. Model Dev., 8, 2465–2513, https://doi.org/10.5194/gmd-8-2465-2015, 2015.
  - Aumont, O., van Hulten, M., Roy-Barman, M., Dutay, J.-C., ÉthéÉthé, C., and Gehlen, M.: Variable reactivity of particulate organic matter in a global ocean biogeochemical model, Biogeosciences, 14, 2321–2341, https://doi.org/10.5194/bg-14-2321-2017, 2017.
- Banse, K.: New views on the degradation and disposition of organic particles as collected by sediment traps in the open ocean, Deep Sea

  Res. A 37, 1177–1195 1177–1195, https://doi.org/10.1016/0198-0149(90)90058-4, 1990.
  - Boyer, T.P., Baranova,O.K., Coleman, C., Garcia, H.E., Grodsky, A., Locarnini, R.A., Mishonov, A.V., Paver, C.R., Reagan, J.R., Seidov, D., Smolyar, I.V., Weathers, K., and Zweng,M.M.: World Ocean Database 2018. A.V. Mishonov, Technical Ed., NOAA Atlas NESDIS 87. https://www.ncei.noaa.gov/sites/default/files/2020-04/wod\_intro\_0.pdf, 2018.
  - Burd, A. B.: Modeling the vertical flux of organic carbon in the global ocean, Annu. Rev. Mar. Sci. 16: 135–61, 2024.
  - Cael, B. B., Cavan, E. L., and Britten, G. L.: Reconciling the size dependence of marine particle sinking speed, Geophysical Research Letters, 48, e2020GL091771. https://doi.org/10.1029/2020GL091771, 2021.
- Cael, B. B. and Bisson, K.: Particle flux parameterizations: quantitative and mechanistic similarities and differences. Front. Mar. Sci., 5,395. https://doi.org/10.3389/fmars.2018.00395, 2018.
  - Cram, J. A., Weber, T., Leung, S. W., McDonnell, A. M. P., Liang, J.-H., and Deutsch, C.: The role of particle size, ballast, temperature, and oxygen in the sinking flux to the deep sea, Global Biogeochemical Cycles, 32, 858–876. https://doi.org/10.1029/2017GB005710, 2018.
- De Soto F., Ceballos-Romero E., Villa-Alfageme M.: A microscopic simulation of particle flux in ocean waters: Application to radioactive pair disequilibrium. Geochim. Cosmochim. Acta 239, 136–158. doi: 10.1016/j.gca.2018.07.031, 2018.
  - DeVries, T., Liang, J. H., and Deutsch, C.: A mechanistic particle flux model applied to the oceanic phosphorus cycle. Biogeosciences, 11, 5381–985381–5398, 2014.
- Druffel, E., Williams, P., Bauer, J., and Ertel, J.: Cycling of dissolved and particulate organic matter in the open ocean, J. Geophys. Res., 97, 15639–1565915639–15659, https://doi.org/10.1029/92JC01511, 1992.
  - Alldredge, A. L., and Gotschalk, C.: In situ settling behavior of marine snow. Limnol. Oceanogr. 33, 339–351. https://doi.org/10.4319/lo.1988.33.3.0339, 1988.
  - Hamby, D. M.: A review of techniques for parameter sensitivity analysis of environmental models, Environ. Monit. Assess. 32, <del>135–154.</del> 135–154.1994
- Jokulsdottir, T. and Archer, D.: A stochastic, Lagrangian model of sinking biogenic aggregates in the ocean (SLAMS 1.0): model formulation, validation and sensitivity, Geosci. Model Dev., 9, 1455–14761455–1476, https://doi.org/10.5194/gmd-9-1455-2016, 2016.

- Kostadinov, T. S., Siegel, D. A., and Maritorena, S.: Retrieval of the particle size distribution from satellite ocean color observations, J. Geophys. Res., 114, C09015, https://doi.org/10.1029/2009JC005303, 2009.
- Kovalets, K., Maderich, V., Brovchenko, I., Seo, S., and Kim, K. O.: KKovalets/EuLag: EuLag (v0.4.0). Zenodo. 550 https://doi.org/10.5281/zenodo.15464336, 2025a.
  - Kovalets, K., Maderich, V., Brovchenko, I., Seo, S., and Kim, K. O.: KKovalets/EuLag\_DataSet: EuLag\_DataSet (v1.0.0). Zenodo. https://doi.org/10.5281/zenodo.15464730, 2025b.
  - Kriest, I. and Evans, G.: Representing phytoplankton aggregates in biogeochemical models, Deep-Sea Res. I, 46, 1841–1859, 1999.
- Kriest, I. and Oschlies, A.: On the treatment of particulate organic matter sinking in large-scale models of marine biogeochemical cycles,

  Biogeosciences, 5, 55–7255–72, https://doi.org/10.5194/bg-5-55-2008, 2008.
  - Lenhart, T., Eckhardt, K., Fohrer, N., Frede, H. G.: Comparison of two different approaches of sensitivity analysis, Phys. Chem. Earth, 27, 645–654. 645–654. https://doi.org/10.1016/S1474-7065(02)00049-9, 2002.
  - Lutz, M. J., Dunbar, R. B., and Caldeira, K.: Regional variability in the vertical flux of particulate organic carbon in the ocean interior, Global Biogeochem. Cycles, 16, 1037, https://doi.org/10.1029/2000GB001383, 2002.
- Maerz, J., Six, K. D., Stemmler, I., Ahmerkamp, S., and Ilyina, T.: Microstructure and composition of marine aggregates as co-determinants for vertical particulate organic carbon transfer in the global ocean. Biogeosciences, 17, 1765–1803, https://doi.org/10.5194/bg-17-1765-2020, 2020.

565

- Maderich, V., Kim, K. O., Brovchenko, I., Kivva, S., and Kim, H.: Scavenging processes in multicomponent medium with first-order reaction kinetics: Lagrangian and Eulerian modeling. Environmental Fluid Mechanics, 21, 817–842. https://doi.org/10.1007/s10652-021-09799-1, 2021.
- Maderich, V., Kim, K. O., Brovchenko, I., Jung, K.T., Kivva, S., and Kovalets, K.: Dispersion of particle-reactive elements caused by the phase transitions in scavenging, Journal of Geophysical Research Geophys. Res., 127, e2022JC019108.https://doi.org/10.1029/2022JC019108, 2022.
- Martin, J., Knauer, G., K., D., and Broenkow, W.: VERTEX: carbon cycling in the northeast Pacific, Deep-Sea Res., 34, 267–285267–285, 1987.
  - McDonnell, A. M., and Buesseler, K. O.: Variability in the average sinking velocity of marine particles, Limnology & Oceanography Limnol.

    Oceanogr., 55(5), 2085–2096. 2085–2096. https://doi.org/10.4319/lo.2010.55.5.2085, 2010.
  - Middelburg, J.: A simple rate model for organic matter decomposition in marine sediments, Geochim. Cosmochim. Ac., 53, <del>1577–1581, doi:</del>1577–1581, https://doi.org/10.1016/0016-7037(89)90239-1, 1989
- Mullin, M., Sloan, P. R., and Eppley, R. W.: Relationship between carbon content, cell volume, and area in phytoplankton, Limnol. Oceanogr., 11, 307–311, 307–311, 1966.
  - Omand, M. M., Govindarajan, R., He, J., and Mahadevan, A.: Sinking flux of particulate organic matter in the oceans: sensitivity to particle characteristics, Sci. Rep. 10, 5582. https://doi.org/10.1038/s41598-020-60424-5, 2020.
- Roca-Martí, M., and Puigeorbé Puigeorbé, V.: Combined use of short-lived radionuclides (<sup>234</sup>Th and <sup>210</sup>Po) as tracers of sinking particles in the ocean, Annu. Rev. Mar. Sci. 16, <del>551–575.</del> 551–575, https://doi.org/10.1146/annurev-marine-041923-013807 2024.
  - Sheldon, R., W., Prakash, A., and Sutcliffe, Jr., W.: The size distribution of particles in the ocean, Limnol. Oceanogr., 17, 327–339327–339,1972.

Siegel, D. A., DeVries, T., Cetini, I., and Bisson, K. M.: Quantifying the ocean biological pump and its carbon cycle impacts on global scales, Annu. Rev. Mar. Sci. 15, 329–356. https://doi.org/10.1146/annurev-marine-040722-115226, 2023.

Smayda, T.: The suspension and sinking of phytoplankton in the sea, Oceanogr. Mar. Biol., 8, 353-414353-414, 1970.

585

Soares, L. M. V, Calijuri, M. C.: Sensitivity and identifiability analyses of parameters for water quality modeling of subtropical reservoirs, Ecol. Modell. 458, 109720, 2021.